CrossMark

Numerical investigation of post-seismic debris flows in the epicentral area of the Wenchuan earthquake

Ni Zhang[1] (ORCID) · Takashi Matsushima[2] · Ningbo Peng[3]

Abstract

Since the 12 May 2008 Wenchuan earthquake, numerous catastrophic debris flows have occurred in the Wenchuan earthquake-stricken zones. In particular, on 14 August 2010, long-duration, low-intensity rainfall triggered widespread debris flows at the epicenter of the Wenchuan earthquake. These flows caused serious casualties and property losses. In this study, a novel approach combining a soil-water mixing model and a depth-integrated particle method is applied to the analysis of the post-seismic debris flows in the epicentral area. The presented approach makes use of satellite images of the debris flow in the affected area. It is assumed that debris source materials are primarily generated from slope failure during the earthquake. Debris flows are initiated after different amounts of cumulative rainfall according to diffusion governing equations. The debris flow disaster is investigated in terms of volume, concentration, discharge, velocity, deposition thickness and affected area by setting the cumulative rainfall, Manning coefficient and diffusion coefficient to 38 mm, 0.1 and 0.004 m^2 s^{-1}, respectively. Although the thickness and volume of debris source materials are underestimated in this study, the numerical results, including the volume concentration, velocity, discharge and the affected area are in good agreement with the actual observations/measurements of the debris flow events. Adopting a simple and efficient numerical model, systematic analysis of the entire debris flow generation process not only contributes to understanding the mechanism of initiation, transportation and deposition, but is also very useful in designing effective protection structures according to the distribution characteristics of the main parameters. Additionally, the coupling effect of multiple debris flows is discussed.

Keywords Post-seismic debris flows · Particle method · Soil-water mixing model · Rainfall · Wenchuan earthquake

Introduction

Mega-earthquakes not only cause serious casualties and property losses but also trigger numerous coseismic geohazards. For

✉ Ni Zhang
  nizhang.961228@gmail.com

  Takashi Matsushima
  tmatsu@kz.tsukuba.ac.jp

  Ningbo Peng
  pengnb10@lzu.edu.cn

[1] International Center for Applied Mechanics, State Key Laboratory for Strength and Vibration of Mechanical Structures, Xi'an Jiaotong University, Xi'an 710049, China

[2] Department of Engineering Mechanics and Energy, University of Tsukuba, Tsukuba, Ibaraki 305-8573, Japan

[3] Faculty of Architecture and Civil Engineering, Huaiyin Institute of Technology, Huaian 223001, China

example, the 12 May 2008 Wenchuan earthquake in China triggered approximately 56,000 landslides (Gorum et al. 2011; Huang and Fan 2013), with a total debris volume of more than 5×10^9 m^3. Extremely abundant loose materials easily serve as source materials for subsequent rainfall-induced debris flows in the earthquake-stricken zones. Since the Wenchuan earthquake, numerous debris flows have occurred in the earthquake-stricken zones in the last ten years (Huang and Li 2009; Fan et al. 2017, 2018), and many of these events have been reported (Xu et al. 2012; Zhang et al. 2016). Investigation of the source material evolution in 11 debris flows occurring during 12–14 August 2010 in the vicinity of Qingping Town in the Wenchuan earthquake area demonstrated that approximately 20% of the landslide deposits evolved into debris flows (Xu et al. 2012). Zhang et al. (2016) noted that the mass transport rates (defined as the percentage volume loss of the hillslope deposits) were 24.5%, 16.3 and 12.1% during the rainstorms in 2010, 2011 and 2013, respectively, by evaluating the evolution of debris flows that occurred after the Wenchuan earthquake along Province Road 303. Therefore, debris flows have

become a dominant disaster type and threaten post-seismic rescue, temporary resettlement, post-reconstruction and rehabilitation in earthquake-stricken zones. Moreover, the post-seismic geohazards effect lasts for several dozens of years (Nakamura et al. 2000; Lin et al. 2003; Huang 2011; Zhang et al. 2016) because of the extreme abundance of loose materials. To prevent and reduce such geohazards, an efficient evaluation of the hazards of post-seismic debris flows shortly after earthquakes in earthquake-stricken zones is very urgently needed.

Previous research (e.g., Tang et al. 2012a; Zhou et al. 2014) concentrated on studying the relationship between the distribution of post-seismic debris flow hazards and their influencing factors, such as earthquake magnitude and intensity, distance from the epicenter, slope angle and material properties, applying a statistical approach based on field data. At present, the field survey is still a typical and primary method of obtaining field data, although it requires considerable manpower and is both time-consuming and inefficient. Moreover, because of a dramatic underestimation of the debris flow hazards during a field survey, many potential debris flow valleys have been overlooked, resulting in an unexpectedly large number of casualties and property losses (Tang et al. 2011a). To efficiently evaluate the potential debris flow valleys, a numerical method considering source materials and rainfall based on an accurate digital elevation model (DEM) is a good choice (Iverson 2014). Nowadays, it is common to numerically evaluate debris flows by incorporating high-resolution satellite images and aerial images into a detailed DEM. Furthermore, debris source materials can also be evaluated using the depth-integrated particle method based on such a detailed DEM (Nakata and Matsushima 2014; Zhang and Matsushima 2018). However, rainfall, one of three essential factors in the generation of debris flows (together with steep topography and sufficient available loose materials; Takahashi et al. 1981), is still uncertain, because of its high variability, especially in mountainous areas.

The rainfall characteristics necessary to trigger debris flows in earthquake-stricken zones have attracted the attention of many researchers. Subsequent to the 1999 Chi-Chi earthquake, the heavy rainfall associated with typhoons resulted in the development of numerous landslides as well as the reactivation of some pre-existing movements. Many non-debris flow catchments before the earthquake evolved into debris flow catchments after the earthquake. Chen and Hawkins (2009) reported the relationships among earthquake disturbance, tropical rainstorms and debris movements. Tang et al. (2015) investigated the catastrophic impact of a debris flow in the Hongchun valley near the earthquake epicenter, revealing that earthquake shaking strongly disturbed the surface strata and that the hillslopes were then conditioned to enhance the likelihood of future landslides and debris flows under heavy rainfall conditions. The corresponding triggering rainfall thresholds and intensity of post-seismic debris flows are significantly reduced in

comparison with the thresholds of pre-earthquake debris flows (Lin et al. 2003; Guo et al. 2016). However, in the Wenchuan earthquake-stricken zones, many valleys with abundant loose source materials did not see debris flows in wet seasons when the rainfall was larger than the threshold (Tang and Liang 2008). One reason is the recordings by rain gage stations cannot reflect the correct rainfall information in the potential debris flow zones, because they are far from research areas and the distribution density of the stations is rather small, particularly in remote, mountainous areas. Another reason is that there are many uncertainties in the initiation process of debris flows, while rainfall is usually taken into account only by the antecedent rainfall account and critical rainfall intensity in an empirical approach (historical, statistical; Zhou and Tang 2014). To a large extent, the rainfall threshold not only has a regional limitation but also varies after successive rain events due to a change in erodible material (Van Asch et al. 2014). How much rainfall is actually used to initiate and transport debris flows? It is necessary to find methodologies capable of identifying the potential debris flow valleys, taking debris source materials and rainfall into consideration, in the earthquake areas in order to provide crucial decision-making information for hazard assessment after an earthquake.

In this study, a soil-water mixing model coupled with a depth-integrated particle method that can efficiently evaluate debris flow hazards by considering deposit entrainment by flow erosion and rainfall characteristics is adopted to analyze the post-seismic debris flows in the Wenchuan epicentral area, based on satellite images.

Geological setting and overview of post-seismic debris flows in the Wenchuan epicentral area

Yingxiu, which is situated in Wenchuan County, Sichuan Province, SW China, is the epicenter of the 2008 Wenchuan earthquake. As illustrated in Fig. 1, Yingxiu Town is located on the Yingxiu-Beichuan fault. With elevation ranging from 880 to 4500 m, the region from Yingxiu to Wenchuan has topography characterized by rugged mountains and incised valleys. The valley density is so large that there are more than 70 valleys with catchment areas ranging from 0.25 km^2 to 55 km^2. Statistically, there are just 16 valleys with areas larger than 10 km^2. Most of these valleys have areas less than 3 km^2. The distance between the valley mouth and the Min River is small and the area outside of the valleys is also so small that the debris flows flow very easily into the river, further blocking its flow (Zhang 2015; Zhang et al. 2016; Ge et al. 2014). Moreover, there are 48 cross angles lying in the range of 80-90° and more than 80% of the cross angles are larger than 70° (Fig. 2). It has been demonstrated that the debris flows have a very high probability of blocking the Min River in this region.

Fig. 1 The epicentral area of the Wenchuan earthquake. The post-seismic images in this region were observed on 31 March 2011. The area enclosed by the red dotted line is the Yingxiu Town; and the black dotted line is the boundary of valleys. The light grey-white zones are areas damaged during the earthquake. The high-elevation zones were covered by snow and cloud, in particular, on the upper right zone of the image
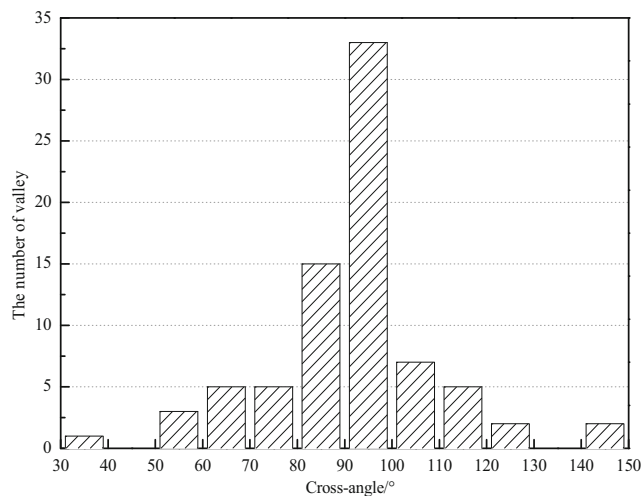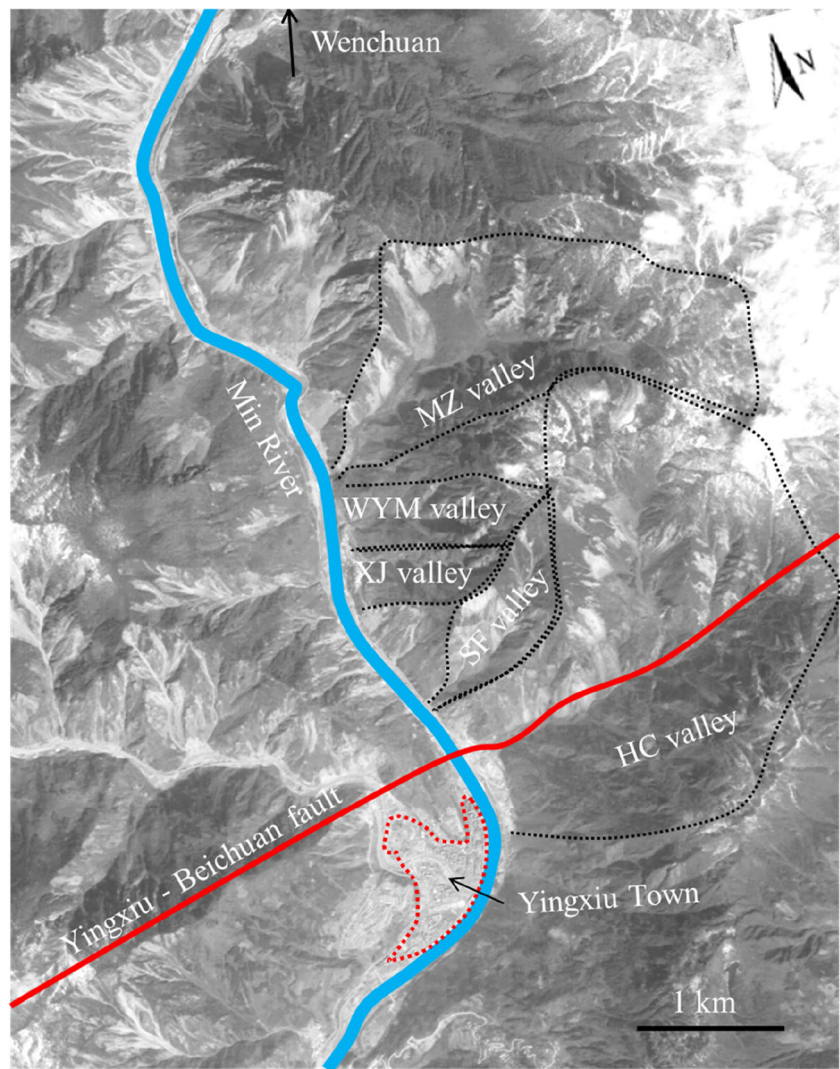
Fig. 2 The cross angles in the region from Yingxiu to Wenchuan along the Min River. A cross angle is defined as the upstream angle between the two intersecting flow lines, i.e., the debris flow and river flow. When the debris flow valleys are perpendicular to the river, the debris flows are very likely to block the river

More than 87% of the slopes have inclinations larger than 20°, while only 10% of the slopes have inclinations larger than 50° (Zhang 2015), according to the 10-m DEM. The mean slope inclination is approximately 37°. The main lithology of this region is pre-Sinian granitic rocks, Sinian pyroclastic rocks, Carboniferous limestone and Triassic sandstone. All bedrock is deeply fractured, heavily weathered and covered with a layer of weathered material (Ge et al. 2014). Loose Quaternary deposits are distributed in the terraces and alluvial fans. After the earthquake, more than 56 new geohazards were identified, compared to the geohazard situation in 2005 in the area from Wenchuan to Yingxiu (Gan et al. 2012). Consequently, more than 0.2×10^9 m^3 of deposits were generated in the area from Wenchuan to Yingxiu along the Min River (Zhuang et al. 2009). The flow direction of the Min River is from Wenchuan to Yingxiu. The annual mean discharge of the Min River is 452 m^3 s^{-1} (Tang et al. 2011a). The annual average precipitation is approximately 1285 mm, with more than 70–80% of it being recorded as part of heavy rainstorms from

June to September. Such heavy rainstorms play a critical role in triggering debris flows.

Since the Wenchuan earthquake, several prolonged rainfalls have triggered many catastrophic debris flows in the earthquake-stricken zones. These debris flows led to many casualties and the destruction of highways, bridges, villages, reconstructed infrastructures and barrier lakes (Ge et al. 2014). In particular, the debris flows on 14 August 2010 killed more than 70 people and all of the 5 debris flows near Yingxiu town flowed into the Min River. As a result, more than half of the riverbed was blocked and the river was pushed to the opposite side, leading to flooding in the newly reconstructed Yingxiu town (Tang et al. 2011a; Xu et al. 2012). Figure 3 shows cumulative rainfall of this debris flow event recorded by the Yingxiu rain gage station marked in Fig. 12. The debris flows in the Yingxiu area occurred on August 14 between 02:00 and 03:00 am, with a critical hourly rainfall of 16 mm h^{-1} and a cumulative rainfall of 106 mm in 10 h. Debris flows usually occur with a combination of high cumulative rainfall and very high rainfall intensity (Crosta 1998). However, cumulative rainfall can reflect actual rainfall initiating debris flow in the physical model. The threshold of rainfall necessary to initiate debris flows in the Yingxiu area is poorly known, though Tang et al. (2011b) reported that small debris flows in branches had already been initiated by more than 60 mm of cumulative rainfall before 02:00 am on 14 August. Previous studies (Tan and Han 1992; Lan et al. 2003) have reported rainfall that initiates debris flows with cumulative rainfall of near 100 mm in southwestern China. Tang et al. (2012b) suggested the expression $I = 25.962\ T^{-0.239}$ (T is rainfall duration) as a rainfall threshold for debris flow occurrence in the Qingping area. Combining the preliminary research and the rainfall

characteristics of the event, three rainfall thresholds ($R1 = 106$ mm, $R2 = 60$ mm and $R3 = 38$ mm) are proposed in this study. In the Results and Discussion section, the cumulative rainfall effect on the initiation of debris flows is analyzed.

Here, the debris flow hazard is evaluated in the epicentral area of the Wenchuan earthquake. In particular, the research area (3.25×4 km; Fig. 1), including five valleys near Yingxiu Town, was selected to numerically investigate the post-seismic debris flows in detail. The basic information for the five valleys (Hongchun, Shaofang, Xiaojia, Wangyimiao and Mozi valley, denoted as HC, SF, XJ, WYM and MZ valley, respectively) is shown in Table 1.

Method and satellite images

Soil-water mixing model coupled with the depth-integrated particle method

Depth-integrated models have been widely adopted to describe erosion and deposition in debris flows (McDougall and Hungr 2005; Hungr et al. 2005; Pastor et al. 2009, 2014; Iverson et al. 2011; Luna et al. 2012; Zhang and Matsushima 2016). The biggest advantage of these methods is their structural simplicity and flexibility. These advantages make it possible to construct a simple, efficient and stable particle method. In particular, Pastor et al. (2009, 2014) developed a smoothed particle hydrodynamics (SPH) model coupled with the depth-integrated model and demonstrated its performance by comparing it with theoretical solutions, laboratory experiments, and disaster case studies. Zhang and Matsushima (2016) proposed a soil-water mixing model

Fig. 3 Cumulative rainfall amount from 13 to 14 August 2010. The debris flow in Yingxiu area occurred on August 14 between 02:00 and 03:00 am with the critical rainfall intensity of 16 mm/h. The red arrow stands for the duration of the debris flow and flood. The flood was observed after 04:00 am on 14 August. Therefore, the cumulative rainfall after 04:00 am will not be used to initiate and generate the debris flow. According to the rainfall characteristic and the preliminary research, three cumulative rainfall of $R1$, $R2$ and $R3$ is proposed to study post-seismic debris flows
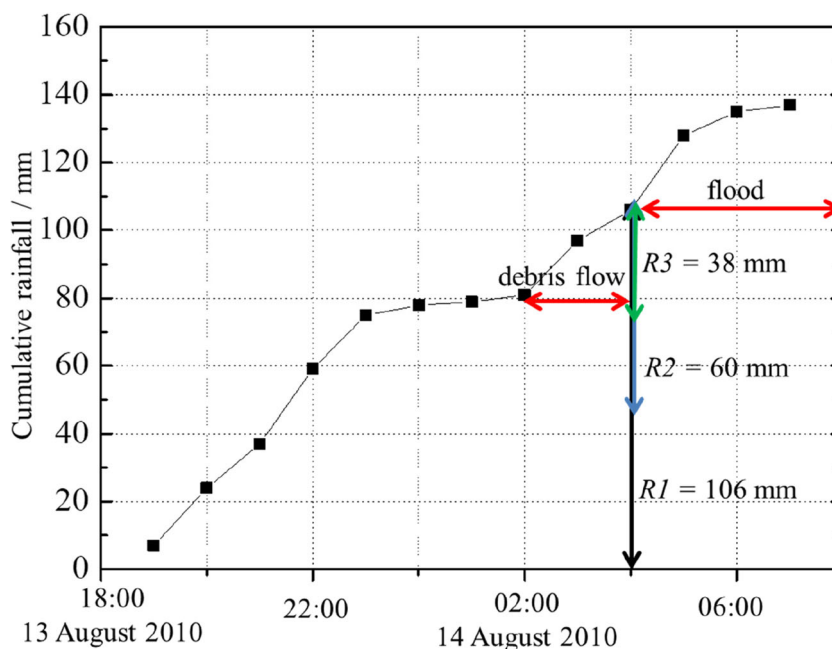
Table 1 The basic parameters of the five valleys in typical research area

Valley name	Catchment area (km²)	Deposition area (km²)	Main channel length (km)	Cross angle (°)
Hongchun	5.2	0.064	3.55	90
Shaofang	0.53	0.018	1.04	101
Xiaojia	0.45	0.012	1.07	99
Wangyimiao	0.4	0.013	1	90
Mozi	5.08	0.01	1.6	90

coupled with the depth-integrated model and demonstrated its performance by comparing the numerical results with theoretical solutions, laboratory experiments, and disaster case studies using actual topographic data. In these Lagrangian particle methods, continuum flow is discretized with numerical particles (or columns) that move along the topographic surface, maintaining information on their material and mechanical properties. Therefore, it is a quasi-3D simulation, and the conservation laws easily hold without dealing with the advection term. However, SPH requires a certain number of numerical particles to assure their accuracy, as well as their computational stability, because of the inherent discontinuity problem at their boundaries. In contrast, a soil-water mixing model coupled with the depth-integrated model is "fully" discretized and is numerically stable. In this study, we focus on introducing the depth-integrated model coupling a soil-water mixing model that can be used to describe the initiation, transportation and deposition of a soil mass.

In the model, we set a horizontal coordinate system, (x, y), and a numerical particle (or column) of soil water mixture whose initial height is h_0 and bottom width is d_0, as shown in Fig. 4. The commonly used shallow water equation [Eq. (1)] is adopted for each particle:

$$\frac{Dv_x}{Dt} = \frac{\partial v_x}{\partial t} + v_x \frac{\partial v_x}{\partial x} + v_y \frac{\partial v_x}{\partial y} = g_x - \frac{\partial p}{\rho \partial x} - \frac{\tau_{bx}}{\rho h}$$
$$\frac{Dv_y}{Dt} = \frac{\partial v_y}{\partial t} + v_x \frac{\partial v_y}{\partial x} + v_y \frac{\partial v_y}{\partial y} = g_y - \frac{\partial p}{\rho \partial y} - \frac{\tau_{by}}{\rho h} \quad (1)$$

where $v = (v_x, v_y)$ is a depth-integrated flow velocity vector, h is the surface height of debris flow, $\tau_b(\tau_{bx}, \tau_{by})$ is the bottom shear stress vector, ρ is the density of the mixture, p is the hydraulic pressure and $g(g_x, g_y)$ is the gravitational acceleration. Note that the mass conservation equation is quite easily described in Lagrangian particle methods as $\rho d^2 h = $ constant.

A particle-wise discretization is adopted for the hydraulic pressure gradient (Fig. 4), which is discretized by the difference in height between the neighboring particles. In this pair-wise particle interaction, the height of each particle is computed from the inter-particle distance by assuming a constant particle volume. Therefore, the pressure is described by the inter-particle distance d [Eq. (2)]. In addition, we assume that the two particles whose distance is 1.5 times larger than the initial particle distance do not interact. The hydraulic pressure is calculated by the following inter-particle force [Eq. (2)].

$$\nabla \mathbf{p} = \rho g \nabla h = \begin{cases} -2\rho g h_0 (1 - \|\mathbf{d}\|/d_0)/(1 + \|\mathbf{d}\|/d_0) \mathbf{d}/\|\mathbf{d}\| & (\|\mathbf{d}\| < d_0) \\ -2\rho g h_0 \left[(\|\mathbf{d}\|/d_0 - 1.25)^2 + 0.0625 \right] \mathbf{d}/\|\mathbf{d}\| & (d_0 \leq \|\mathbf{d}\| < 1.5d_0) \\ 0 & (\|\mathbf{d}\| \geq 1.5d_0) \end{cases} \quad (2)$$

where d is the distance vector between two interacting particles.

The bottom shear stress is expressed based on the Manning equation as follows:

$$\tau_b = \left(\tau_{cr} \|v\|^m + \rho g \frac{n^2}{R_h^{1/3}} \|v\|^2 \right) \frac{v}{\|v\|} \quad (3)$$

$$\tau_{cr} = \rho g R_h i_{cr}$$

where n is the Manning coefficient, R_h is the hydraulic radius, i_{cr} is the critical slope angle of deposition, and m is a numerical parameter. In the present study, m is set to 0.01, considered as a sufficiently small value to reproduce the Bingham type

response and a sufficiently large value to assure the efficiency of the numerical computation (Zhang and Matsushima 2016).

There are only two major parameters in the depth-integrated particle model to control the flow behavior: the Manning coefficient and the critical slope of deposition. To couple the depth-integrated particle method and the soil-water mixing model, the diffusion equation [Eq. (4)] is adopted.

$$c(\mathbf{d}, t) = (4\pi D t)^{-1/2} e^{-\mathbf{d}^2/4Dt} \quad (4)$$

where c is the volume concentration of each particle and D is the diffusion coefficient. Another very important aspect of the model is to link the soil volume concentration c to the
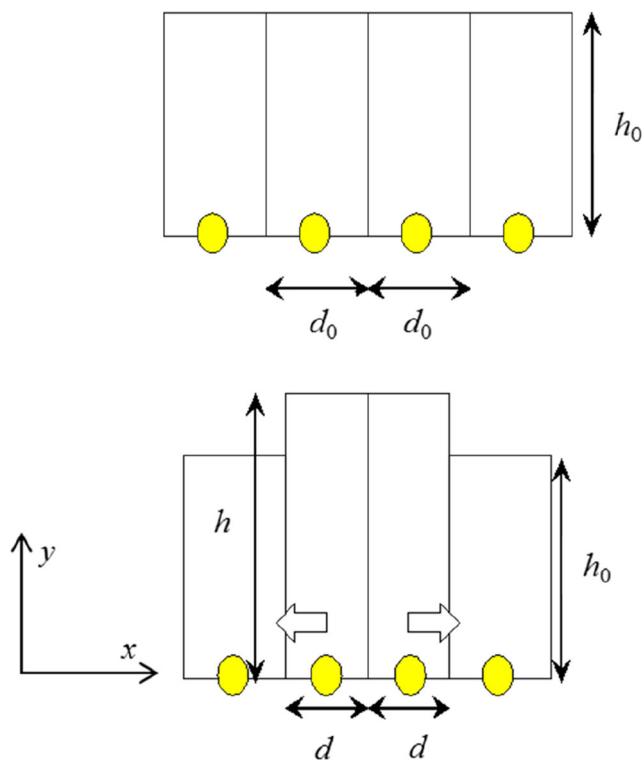
Fig. 4 Particle interaction model based on hydraulic pressure gradient. The yellow dots are particles in the model. h_0 and d_0 are the initial dimensions of the column, and the h and d are the dimensions of column after deformation

mechanical properties. The condition $c = 0$ indicates that the material is water, while $c = 1$ corresponds to dry soil. Therefore, the critical slope angle of deposition, i_{cr}, can be set as a function of c such that $i_{cr}(c = 0) = 0°$ and $i_{cr}(c = 1) = i_m$, where i_m is the repose angle of the soil material in the dry condition. Zhang and Matsushima (2016) proposed the following two-parameter smooth function between the above two extreme conditions:

$$i_{cr} = i_m\left(1/1 + e^{-\alpha(c-c_m)} - 1/1 + e^{\alpha c_m}\right) \qquad (5)$$

where c_m is the critical concentration for the transition between the soil phase and water phase and α is a numerical parameter to describe the change rate of the critical failure slope. Regarding c_m, some field observations suggest that the critical concentration is approximately 0.83 (Fei and Shu 2004), while no information is available for α. As a result, c_m and α are set to 0.8 and 20 in the present study, respectively. According to the preliminary study, these parameters are not very influential to the simulation results in comparison with the effects of i_m and D (Zhang and Matsushima 2016).

In the model, two main physical parameters need to be determined, the Manning coefficient and the diffusion coefficient. The Manning coefficient has been widely used in the field of river engineering (Limerinos 1970), providing

the suggested values of water flow on floodplains (0.07 to 0.10 for medium to dense brush and 0.15 for trees; Chow 1959) and on natural channels (0.060 to 0.075; Barnes 1967), and the suggested values of debris flow in valleys (0.01–0.1 for a relatively stable valley channel, and 0.1–0.5 for rougher and steeper valley channels; Chen and Zhang 2006). In the actual soil-water mixing process, D controls how fast the soil mass is exchanged between the two neighboring particles. It must be a function of velocity fluctuation, soil type, the condition of the deposition, etc. In the present study, however, we assume it as constant because currently we do not have the quantitative relationship between D and its influential factors. By comparing the numerical results and the laboratory experiments, the valid range of the coefficient D is found to be 0.0006– 0.005 m^2 s^{-1} (Zhang and Matsushima 2016).

To apply the soil-water mixing model to the valley bottom soil erosion and the volume increase of the debris flow, a two-step simulation procedure is adopted. In the first step, according to the critical failure slope angle and repose angle of the materials in the study area, dry slope failure is simulated to prepare numerical particles of loose soil deposit with $c = 1$. Then, in the second step, numerical particles representing rainfall are generated in the entire research region, including the solid material generated in the first step. During the process of rainfall, particles flow down and form surface runoff under a gravitational force, and solid particles are mixed by exchanging soil mass according to the diffusion equation. This process causes the change in i_{cr} for loose soil deposit particles and the change in their mobility, and finally, generates a debris flow and further flows together as a larger debris flow.

Satellite images

The Advanced Land Observing Satellite (ALOS) was in operation from 24 January 2006 to 12 May 2011. The ALOS was expected to contribute to society in numerous ways, such as cartography, regional observation, disaster monitoring and resource surveying. The ALOS has three remote sensing instruments: PRISM, AVNIR-2 and PALSAR. To compare and analyze the affected area and deposits, we obtained pre- and post-seismic satellite images in the epicentral area from the PRISM sensor. The detailed information from the images is shown in Table 2. The covered area per image from the PRISM sensor is 70 × 35 km. The spatial resolution of the satellite images is 2.5 m. Considering the computational capacity and simulation time, a 10-m DEM were processed from the pre-seismic satellite image to supply accurate topographic information for simulating deposits and debris flows, while the post-seismic images from the PRISM sensor were used to analyze the numerical results.

Table 2 The information of satellite images in the epicentral area of Wenchuan earthquake

Scene ID	Obs. date	Product ID	Img_Center coordinate		Img_Cloud quantity	Note
			Lat.	Long.		
ALPSMB072073030	20,070,602	O1B2R_UB	31.082	103.635	4	Pre-seismic
ALPSMW072072975	20,070,602	O1B2R_UW	31.068	103.628	5	
ALPSMB119043025	20,080,419	O1B2R_UB	31.362	103.538	5	
ALPSMN119042970	20,080,419	O1B2R_UN	31.347	103.531	5	
ALPSMW219692975	20,100,310	O1B2R_UW	31.068	103.627	1	Post-seismic
ALPSMB219693030	20,100,310	O1B2R_UB	31.111	103.485	2	
ALPSMB219693025	20,100,310	O1B2R_UB	31.359	103.550	2	
ALPSMW219692970	20,100,310	O1B2R_UW	31.315	103.692	2	

Results and discussion

In this section, the soil-water mixing model coupled with the depth-integrated particle method is applied to evaluate post-seismic debris flows in the epicentral area of the Wenchuan earthquake. Numerical investigations of debris flows in the study area are performed: (1) the spatial distribution of debris source materials is investigated, and evaluated in comparison with the post-seismic satellite images; (2) the numerical simulations considering the entrainment of deposits into debris flows are carried out; and (3) coupling effects between multiple debris flows are discussed.
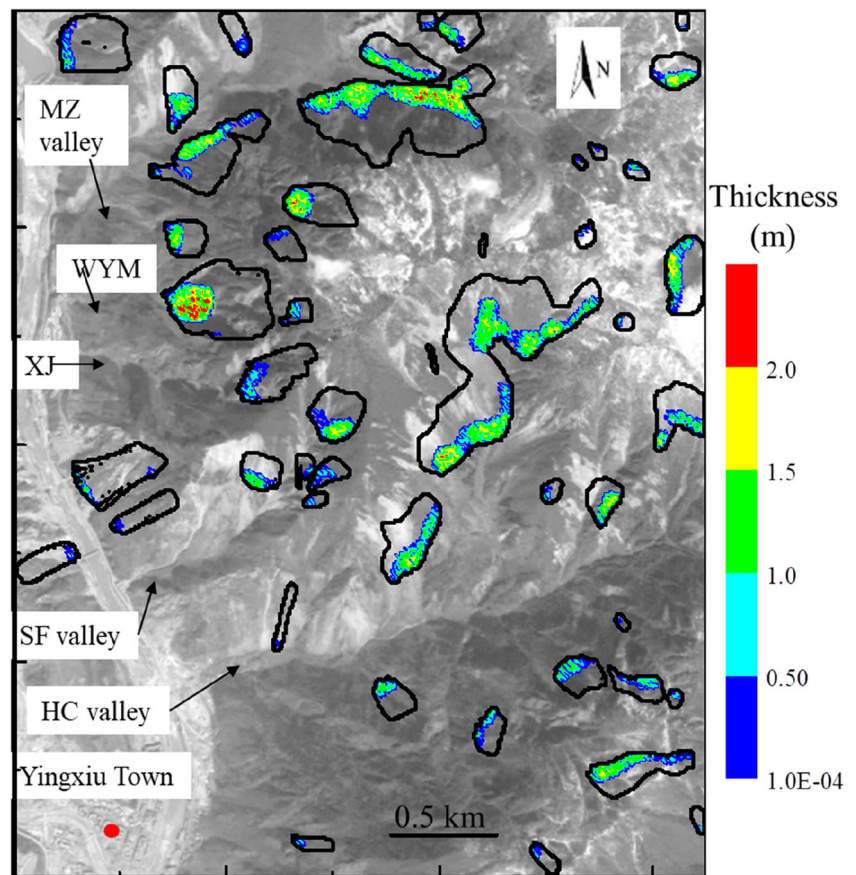
Debris source materials

The 2008 Wenchuan earthquake triggered numerous landslides, leaving a large amount of loose materials on the hillslopes and channels (Xu et al. 2014). Although this region sees many ancient debris flows and has considerable loose deposits on both sides of the channels, the new deposits formed during the earthquake are still dominant in the study area. All the deposits are considered potential source materials for debris flows. Under a seismic wave, the topographical slope serves as the main factor controlling the development of coseismal geohazards. By field survey, Huang (2011) observed that the inclination of the failed slopes ranged from 10 to 70°; in particular, more than 85% of the unstable slopes had an inclination from 20 to 50°. By interpreting satellite images, Tang et al. (2011a) found that 75% of the coseismic landslides occurred in locations with slopes between 30 and 50°. In this study, unstable debris source materials are generated from shallow landslides with relatively steep slopes with inclinations larger than 37° by parametric studies (Zhang 2015). First, unstable slope areas with steep slopes with inclinations larger than 37° are determined from the topographic data, and debris 'particles' are assumed to be positioned there. Then, those particles flow down the slopes and heap up at the valley bottom. In the present study, the repose angle of loose deposits is set to 30°, which is the typical repose angle of dry sand. The Manning coefficient is set to 0.1 following Chen and Zhang (2006), and the initial particle height is assumed to be 1.0 m. The volume concentration of all particles is 1 in this step.

Figure 5 shows the distribution characteristics of the debris source material. There are 49 sites with generated source materials in the 5 valleys. By calculating the slope failure area and deposition area, the affected area is approximately 18% of the study area. In particular, two larger valleys have larger damaged areas (the area enclosed in the black line in Fig. 5), 22 and 15 sites for the HC and MZ valley, respectively. In the HC valley, the source materials are mainly distributed upstream of the valley. Moreover, debris materials in the HC valley are distributed on the left side of main valley channel (hanging wall) due to the hanging wall effect from the Wenchuan earthquake (Donahue and Abrahamson 2014). In the MZ valley, the main source materials are distributed at the middle of and downstream along both sides of valley channel. Compared with the base images, our numerical simulation gives a quite similar affected area. The mean deposition thickness of debris source materials is approximately 1.5 m and the largest thickness is up to 2.5 m. The total volume of debris source materials is 564,000 m^3. Tang et al. (2011a) evaluated the mean thickness and volume of deposits by analyzing the aerial photographs and found them to be 5.5–7.2 m and 1,032,000 m^3, respectively. In their study, the depth of landslides was obtained using a regression analysis between the landslide surface area and the landslide depth based on 62 field measurements. The simulated values of volume and thickness for deposits are clearly smaller than the evaluation results of Tang et al. (2011a). This implies that the assumed thickness of 1.0 m might be smaller than the actual deposition thickness.

Although the thickness and volume of debris source materials are smaller than that indicated by the field data in

Fig. 5 The simulation results of debris source materials. The enclosed areas in black curves are the shallow landslides with relatively steep slopes with inclinations larger than 37°. The debris source materials are mainly distributed on the hillslopes and valley channels. The colorful areas are the deposits generated by the shallow landslides, and the legend shows the thickness of deposits. The base image is satellite image observed by the ALOS on 10 March 2010; the light grey zones, except the summit, are areas damaged during the Wenchuan earthquake

comparison of the preliminary research, the spatial distribution of source materials agrees well with post-seismic satellite images. This infers the probability of performing deposit identification by slope failure without the field investigation. This finding is quite important for the hazard assessment of a relatively large area shortly after an earthquake, because it is hard to reach and perform thorough field investigations in mountainous areas. Obtaining the thickness of deposits from images remains a challenge.

Debris flows

Rainfall is another important factor to be evaluated before conducting the debris flow simulation. The observed cumulative rainfall is 106 mm in 10 h and the critical hourly rainfall is 16 mm h^{-1} (Fig. 3). The critical hourly rainfall is an index used to predict the possibility of debris flow occurrence, but its value cannot be used to initiate the debris flows in a physical model. Before the critical rainfall intensity triggers debris flow, there must be enough cumulative rainfall to soften and weaken soils by infiltration. However, how much antecedent rainfall is actually required to initiate debris flows can be modeled. According to the rainfall characteristics and previous studies (Tan and Han 1992; Lan et al. 2003) in a neighboring region, three

cumulative rainfall values ($R1$ = 106 mm, $R2$ = 60 mm and $R3$ = 38 mm; Fig. 3) are proposed in this study to generate debris flows. The rainfall particles are distributed averagely in the study area, including the debris source materials, which are generated in the first step. The deposits are rather loose shortly after an earthquake and are easily transported with rainfall. Therefore, it is reasonable to set a larger value for the diffusion coefficient ($D1$ = 0.004 and $D2$ = 0.001). To explore the trade-offs between the model parameters and their effects on entrainment, six cases (case 1–case 6; Table 3) with varying cumulative rainfall and diffusion coefficients are preliminarily studied by assuming uniform rainfall in the research area.

The entrainment rate is defined as the percentage volume loss of debris source materials. By simulating six cases, it is found that the entrainment rate clearly varies with cumulative rainfall and diffusion coefficient. Moreover, the entrainment rate decreases with decreasing cumulative rainfall and diffusion coefficient. In case 1, the entrainment rate is so high that more than 70% of debris source materials flow out from the valleys if the diffusion coefficient is set to 0.004, assuming antecedent cumulative rainfall is completely required to initiate and transport debris flows. Under the same rainfall conditions, the volume of debris source materials by entrainment is reduced by

Table 3 The parameters of a series of simulations in the preliminary study

Cases	Cumulative rainfall (R, mm)	Diffusion coefficient (D, $m^2\ s^{-1}0$)	Mean entrainment rate (%)
Case 1	$R1 = 106$	$D1 = 0.004$	70
Case 2	$R1 = 106$	$D2 = 0.001$	56
Case 3	$R2 = 60$	$D1 = 0.004$	57
Case 4	$R2 = 60$	$D2 = 0.001$	41
Case 5	$R3 = 38$	$D1 = 0.004$	43
Case 6	$R3 = 38$	$D2 = 0.001$	36

approximately 14% at a smaller diffusion coefficient, compared to a larger diffusion coefficient in case 1. When the cumulative rainfall is set to 60 mm, the entrainment rate is 57 and 41% at diffusion coefficients of 0.004 and 0.001, respectively. If the cumulative rainfall is 38 mm, the entrainment rate ranges from 36 to 43% when the diffusion coefficient is set to 0.001–0.004. It is interesting that the entrainment rate is rather close in both case 2 ($R1 = 106$ mm, $D2 = 0.001$) and case 3 ($R2 = 60$ mm, $D1 = 0.004$), approximately 56%, and both case 4 ($R2 = 60$ mm, $D2 = 0.001$) and case 5 ($R3 = 38$ mm, $D1 = 0.004$), approximately 43%. It is inferred that a constant entrainment rate can be obtained either by increasing rainfall with a small diffusion coefficient or increasing the diffusion coefficient with less rainfall. The entrainment rate is a variable of a larger region that includes multiple debris flow valleys. From field surveys at many sites in the HC valley, the entrainment rate is approximately 22%.

However, in some local areas it can be up to 64% (Tang et al. 2011b).

To a large extent, the cumulative rainfall and diffusion coefficient not only control the entrainment rate but also influence the volume concentration, which further determines the possibility of formation of a debris dam in the river. Figure 6 shows the distribution characteristics of the volume concentration at the final state of HC deposition zone for case 4, case 5 and case 6. In these three cases, the volume concentration of the debris flow deposits is up to 0.7 in the center of the deposition zone. Among the three deposits of debris flow, the volume of deposits in case 4 is the largest one, case 6 is the smallest one, and case 5 is between case 4 and case 6. However, the volume of deposits with relatively high concentration (larger than 0.5) in case 5 is the largest among the three cases, while the case 6 is the smallest. A debris flow with a larger volume and a higher concentration is more likely to block the river. Therefore, the debris flow in case 5 has
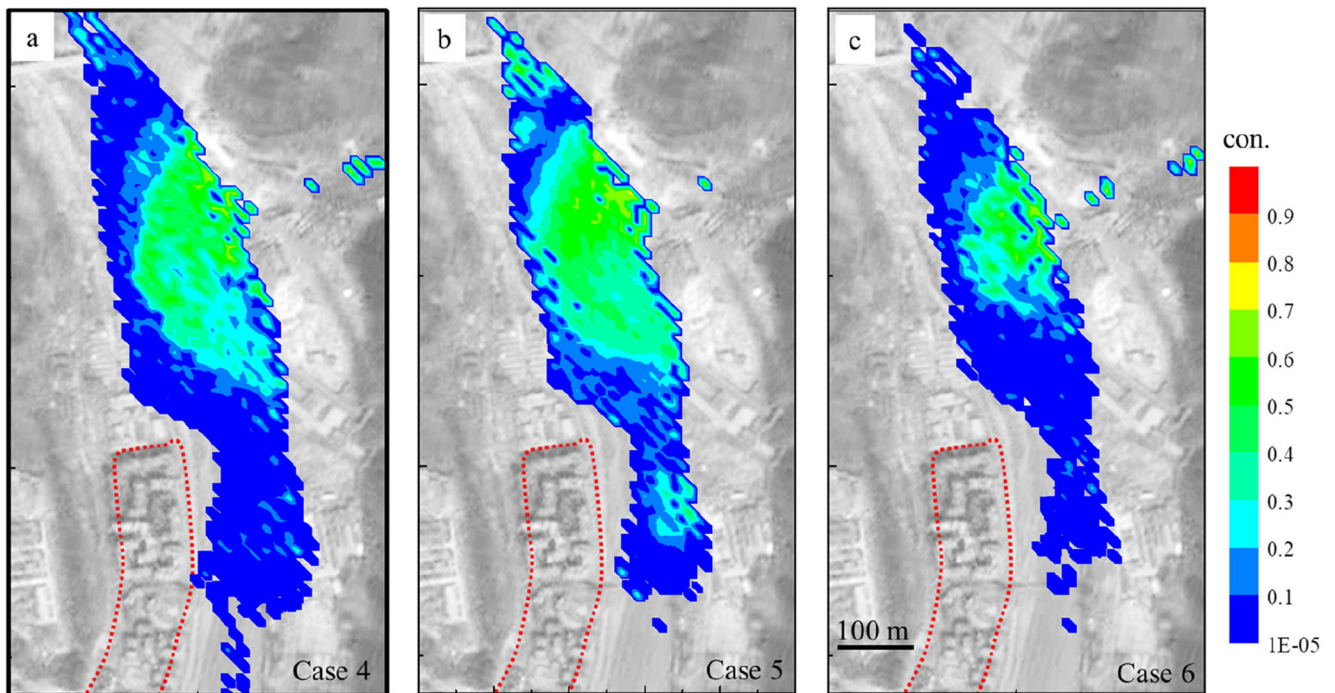
Fig. 6 The volume concentration distribution characteristic on the HC deposition zone at the final state for different cases: case 4 ($R2 = 60$ mm, $D2 = 0.001$), case 5 ($R3 = 38$ mm, $D1 = 0.004$) and case 6 ($R3 = 38$ mm, $D2 = 0.001$). The area in red dot line is the newly reconstructed Yingxiu Town

the highest possibility of forming a debris dam and blocking the river. Actually, the debris flows in the HC valley formed debris dams and partially blocked the Min River (Gan et al. 2012).

By evaluating the entrainment rate and the volume concentration in the HC deposition zone, the numerical results from case 5 agree best with the actual events in comparison with the field investigation. Therefore, the detailed numerical results (volume, concentration, velocity, discharge and affected area) of case 5 will be discussed to evaluate post-seismic debris flows in the Wenchuan epicentral area.

First, the debris flow volume is investigated. It is controlled by the surface runoff, the volume of deposits and the diffusion coefficient for given topographic conditions. The surface runoff is determined by the valley area because uniform rainfall is assumed in the simulations. Rainfall particles flow down according to the equation of motion, and form runoff based on the given topographic characteristics. The runoff can erode solid materials and entrain them along the flow path according to the diffusion equation. Initially, the increase in debris flow volume mainly originates from the mixing between hillslope deposits and surface runoff. During the surface runoff and/or debris flow moving process, the volume rapidly increases due to the entrainment of channelized sedimentation along the flow path. Gradually, the channelized debris flows, replacing the hillslope debris flows, become the dominant flow type. The volume of these 5 debris flows transported into the river are 100,000 m^3, 20,000 m^3, 10,000 m^3, 10,000 m^3 and 150,000 m^3 in the HC, SF, XJ, WYM and MZ valleys, respectively. From the field survey, debris flows of approximately 400,000 m^3 flowed into the Min River from the HC valley. The numerically obtained volume is smaller than that from the field data, probably due to the smaller volume of debris source materials generated in step 1.

Second, Fig. 7 shows the distribution map of volume concentration in the flowing process. With the diffusion effect between source materials and surface runoff, the volume concentration of particles is reduced and the debris flows are initiated. The three smaller debris flows (SF, XJ and WYM) reach the river first, due to the shorter channel lengths, and start depositing with a mean concentration close to 0.3. At the same time, the other two larger debris flows (HC and MZ) flow towards the deposition fan. After 400 s from initiation, the debris flow in the MZ valley starts to deposit in the deposition zone with a mean concentration of approximately 0.6, whereas the debris flow in the HC valley flows out of the valley mouth with a low concentration in the front (Fig. 7b). Compared with the evolution characteristic of the concentration in Fig. 7a, b, c and d, the volume of the high-concentration deposits on both sides of debris flow over time is reduced. Hillslope deposits upstream of both larger valleys move down to the channels and become entrained in both sides of the valley channel due to erosion and bank failure.

Due to the deposit entrainment along the entire flow path, the concentration varies at different sites and stages (Fig. 7a, b, c and d). Finally, the concentration in the MZ valley is about 0.7, while the concentration is close to 0.6 in the HC valley. In the actual debris flow event, the five deposition zones were formed (Tang et al. 2011b; Xu et al. 2012). The concentration was near 0.6 for the HC debris flow by measuring the bulk density of the debris flow (Tang et al. 2011b).

Third, the velocity of the debris flows is investigated. Figures 8a and b show the velocity distribution map at two times ($t = 400$ s and 500 s). The velocity varies with topographic features at different stages. The maximum velocity is approximately 7 m s^{-1}. The velocity is about 4 m s^{-1} when the debris flow runs into the river. This velocity largely determines whether a debris dam forms. The velocity also influences the destructive power and impact force. By field measurement of mud lines and empirical estimation, the velocity ranges from 5.2 to 13.2 m/s by assuming the Manning coefficient ranges 0.05 to 0.067 for the HC debris flow (Li et al. 2012). However, Gan et al. (2012) and Tang et al. (2011b) evaluated the velocity near the HC valley mouth to be approximately 8 m/s. The simulation value is in the range of the field data. Such simulation results are very useful in designing effective protection structures to avoid large debris flows arriving simultaneously at the main channel.

Next, the deposition thickness of the debris flow at the final state is calculated in Fig. 9. The deposits distributed in the river channel are mainly debris flows, while the deposits distributed on the slope surface and valley channel are mainly remaining debris source materials. The mean deposition thickness of the debris flow is approximately 1.5 m, and the largest thickness is near 4 m in the MZ deposition zone. Preliminary research (Tang et al. 2011b; Xu et al. 2012) indicated that the thickness of deposits in the river by the HC valley was 9 m. The simulated result is much smaller than the observed value, because the thickness and the volume of debris source material in the simulation were significantly smaller than the measured values.

Figure 10 shows the hydrograph for four cross sections (HC01, HC02 for the HC valley; MZ01, MZ02 for the MZ valley) and the peak discharge in the HC debris flow was 286 m^3 s^{-1} according to the field investigation (Li et al., 2012). The sites of the cross sections are shown in Fig. 8b. Comparing HC01 and HC02, although the shape of hydrograph is different, the peak discharges are almost identical. A peak discharge of approximately 300 m^3 s^{-1} is observed in HC01 and HC02. Some deposits are entrained into the main debris flow from HC01 to HC02 before the peak discharge in HC01 moved to HC02. The shape of the hydrograph in the MZ valley is completely different. At MZ01, the hydrograph has only one peak value, while there are two peaks at MZ02. The peak discharge at MZ01 is clearly smaller than the peak discharges at MZ02. At MZ02, the first

Fig. 7 The volume concentration distribution characteristics of case 5 ($R3 = 38$ mm, $D1 = 0.004$) at different stages
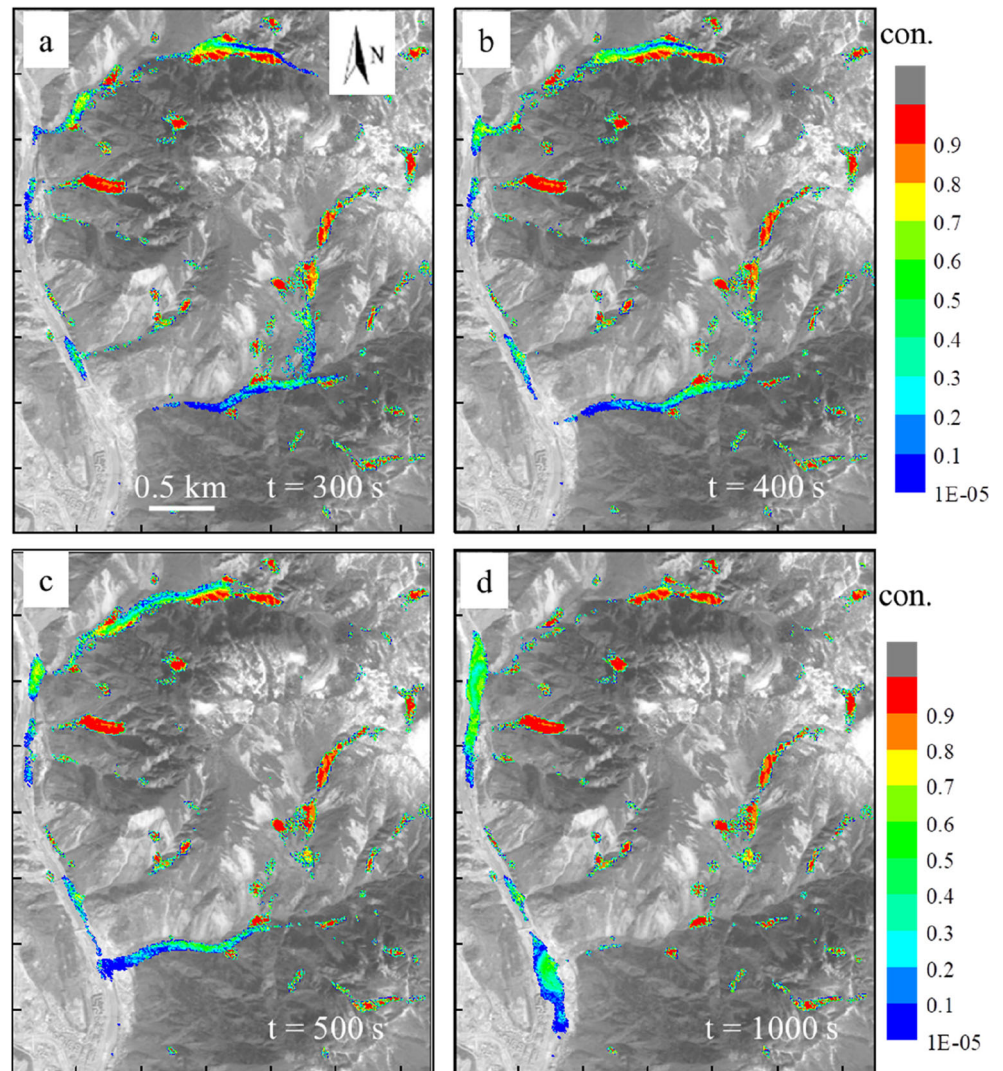
peak discharge demonstrates that many deposits located in zones from MZ01 to MZ02 are entrained into the debris flow and form the first surge in the MZ debris flow; the second peak discharge indicates that the second surge is mainly generated from the upstream flow. The peak discharge is approximately 550 m^3 s^{-1}, which is larger than the water discharge of the Min River [452 m^3 s^{-1} by Tang et al. (2011a)]. This might be one of the main reasons that debris flows partially blocked the river. Fortunately, the two surges in the MZ valley did not coincide in time; otherwise, they would have caused more serious hazards.

Finally, the affected area (including the initiation zone, the transportation zone and the deposition zone) is investigated. The distribution of the affected area is largely determined by the location of the debris source materials as well as the runoff characteristic. As illustrated in Fig. 11, in the three smaller valleys, the affected area is mainly distributed along the valley channels, while the hillslope is also affected in the two larger valleys. All of the five debris flows

partially bury highways and block the Min River. In practical situations, engineers usually pay more attention to the deposition zone where serious damage is caused. It is necessary to do hazard assessments in the deposition areas in detail in order to protect people and infrastructure from future debris flows and to manage the risk more effectively (Hürlimann et al. 2006; Prochaska et al. 2008). Therefore, the area affected by the HC debris flows is analyzed in detail, because the HC debris flow directly threatens the safety of Yingxiu Town. As shown in Fig. 12, the range of the affected area is marked in red. A large amount of debris flows flow into the Min River and partially block it. Consequently, the river course is forced to move to the opposite side and the newly rebuilt town is seriously flooded. It seems that the affected area is slightly larger than the actual damaged area (Fig. 12), ignoring the volume of deposits underwater. If the affected area with high-concentration deposits is compared with the actual deposits, the affected area should agree well with the actual deposition range.
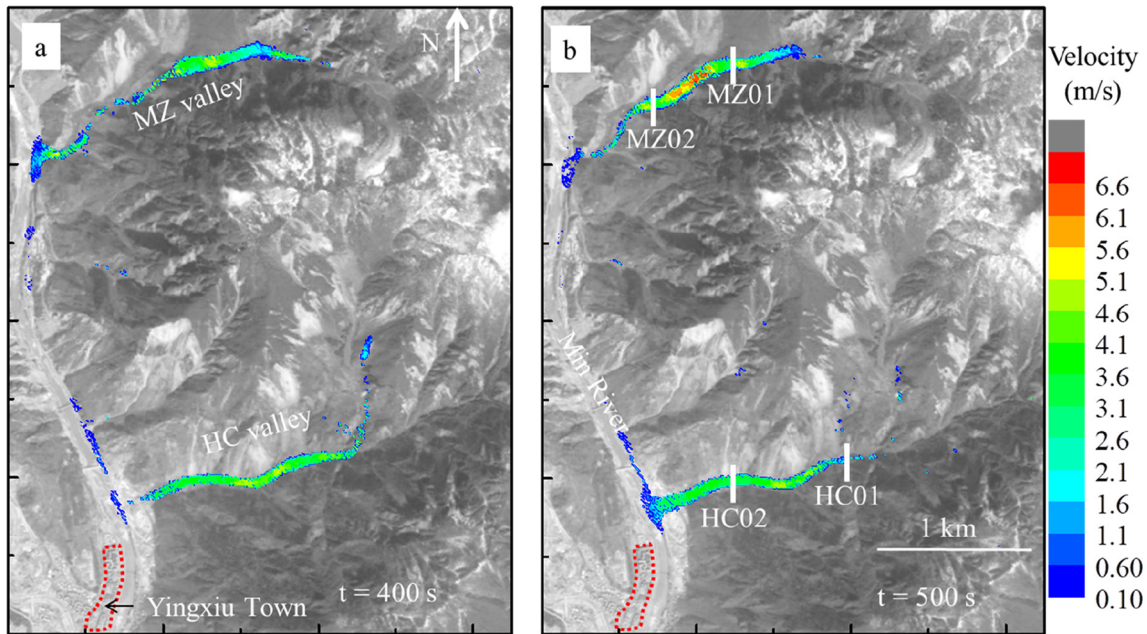
Fig. 8 The velocity distribution characteristics of case 5 ($R3 = 38$ mm, $D1 = 0.004$) at different stages. The area within the red dotted line is the newly reconstructed Yingxiu Town. Four cross sections, HC01, HC02, MZ01 and MZ02, are selected to evaluate some parameters of debris flows, such as maximum velocity and peak discharge.

Although the thickness and volume of debris source materials are underestimated in the study, the volume concentration, velocity, discharge and affected area are well simulated by setting the lowest cumulative rainfall to 38 mm and a larger diffusion coefficient to 0.004. However, the volume and deposition thickness of the debris flow are markedly smaller

**Fig. 9** Deposition thickness of the debris flows at the final state
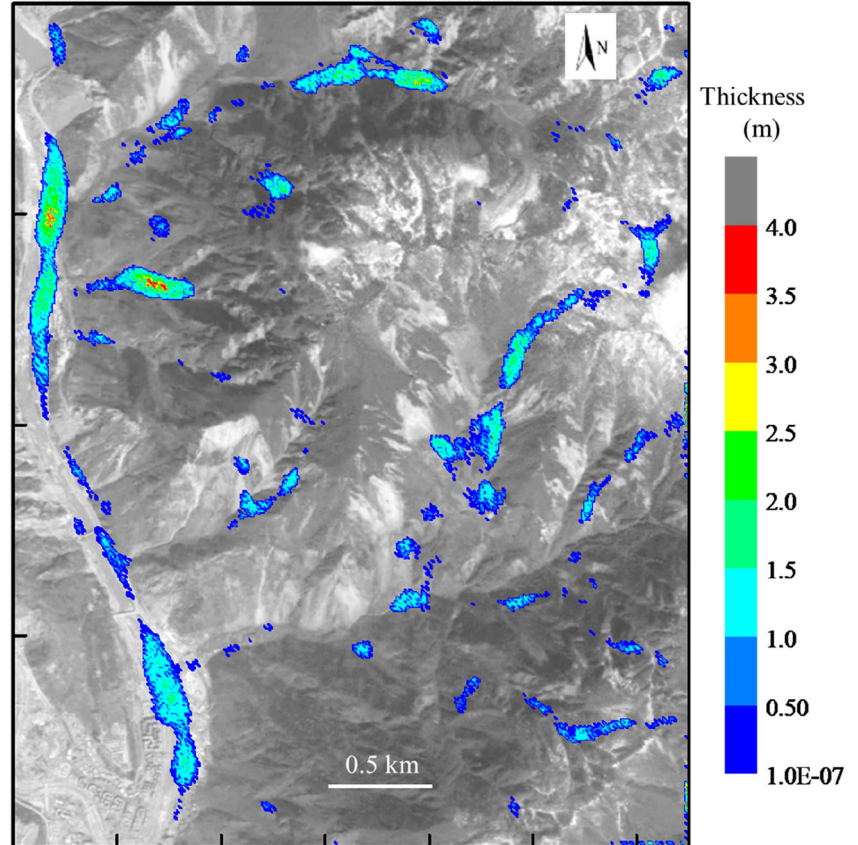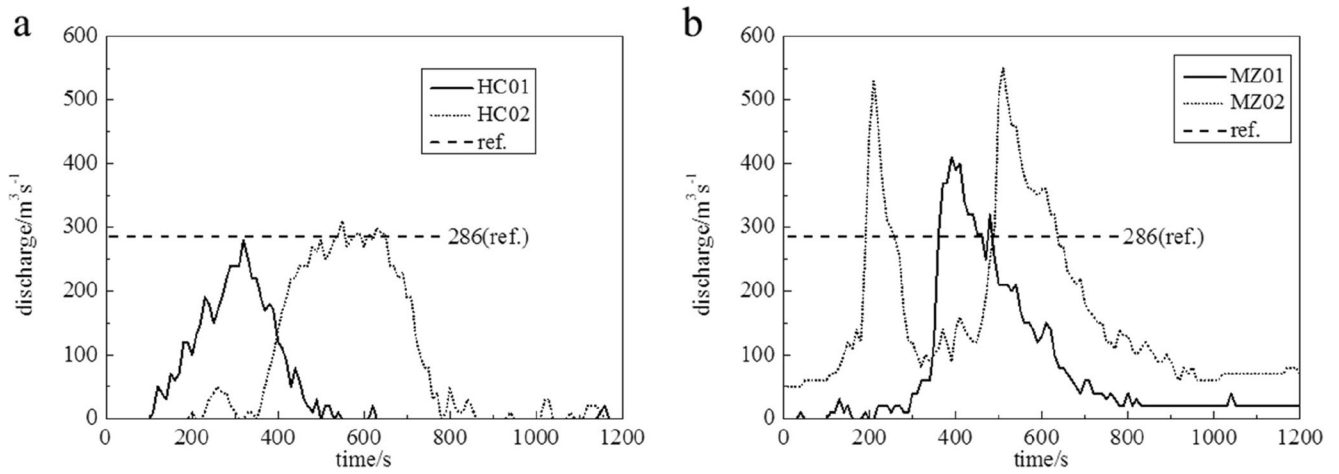
Fig. 10 The hydrograph for the HC and MZ debris flows. HC01 and HC02 are two selected cross sections in HC valley, while MZ01 and MZ02 are two selected cross sections in MZ valley; the corresponding locations are shown in Fig. 8b. The dashed line 286 (ref.) means that the peak discharge in the HC debris flow was estimated as 286 m^3 s^{-1} by Li et al. (2012), according to field investigation

than the observed values. This demonstrates that the volume and deposition thickness of debris flows are largely determined by the volume of debris source material and cumulative rainfall, because more debris materials must be initiated by more rainfall. Additionally, the cumulative rainfall in the actual event must be larger than 38 mm.

Fig. 11 Simulated results of the affected area in study area
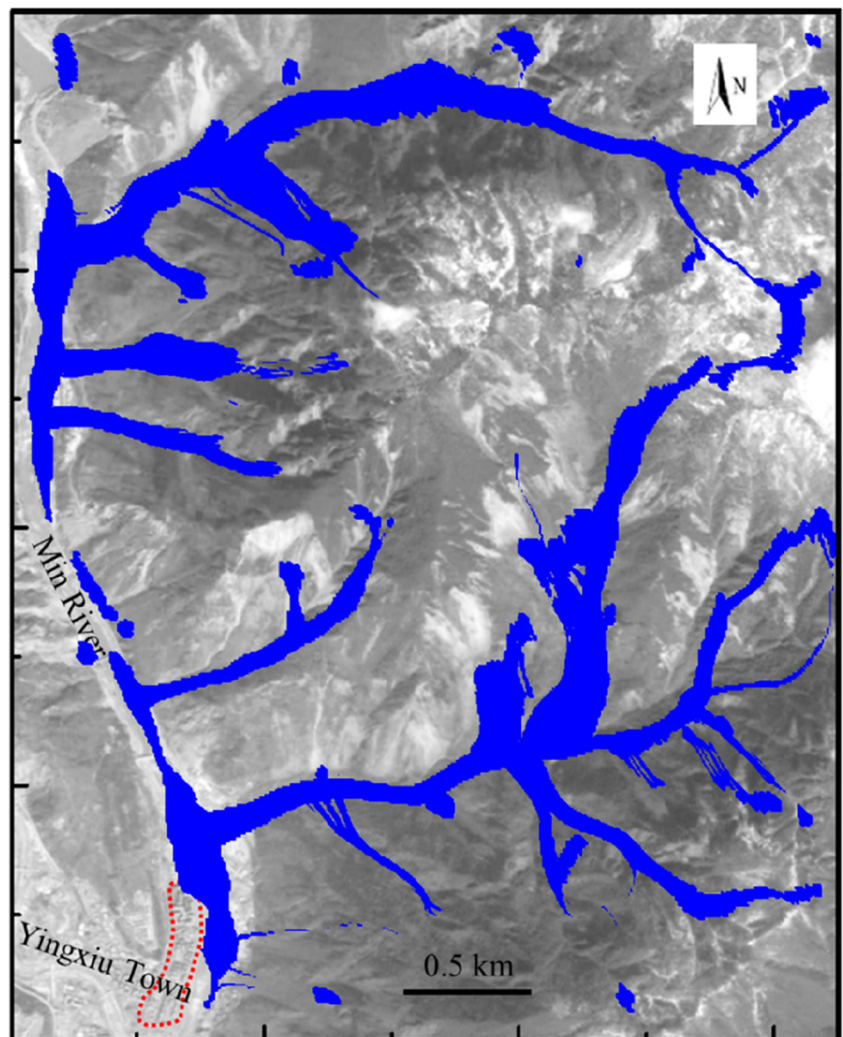
Fig. 12 The area affected by HC debris flow on the deposition zone. The base image is from Tang et al. (2011a, 2011b), an aerial photo taken on 15 August 2010 showing the HC debris flow fan, and the inundated area in the newly reconstructed Yingxiu town within the yellow dash line. The range within the red line is the simulation results of affected area by the HC debris flow on the deposition zone

Coupling effects between multiple debris flows

Multiple debris flows, which will be more likely to occur simultaneously is a typical characteristic of post-seismic debris flows in earthquake-stricken areas during heavy rainstorms (Lin et al. 2003; Okano et al. 2012; Jeong et al. 2011; Sepúlveda et al. 2015). Consequently, the coupling effect between multiple debris flows increases the complexity of the hazards and induces additional difficulty in the analysis (Chen et al. 2016). In this study, there are two kinds of interactions between multiple debris flows in space during a rainfall event. One occurs within one valley with multiple branches (e.g., HC debris flow), while the other occurs in the deposition zone among debris flows from different valleys (e.g., the coupling between HC debris flow and MZ debris flow in the river). In the HC valley, debris flows derived from multiple branches merge and result in different flow properties (Figs. 7, 8 and 9). In the study area, due to multiple debris dams formed in the river, the possibility of blocking the river increases. In particular, the upstream section of the MZ debris flow forms a debris dam earlier than the HC debris flow, and the MZ flow has a larger volume concentration (Fig. 7b and c). The

sequence of successive debris flows significantly influences the runout characteristics of the debris flows (Chen et al. 2016). The deposits in the MZ deposition zone partially blocked the river. The cross section of the river flow and its discharge are reduced. Therefore, the formation of the MZ debris dam makes it easier for the HC debris flows to block the river, to a large extent. The discharge and volume concentration are two good indices to evaluate such a coupling effect. In a practical situation, the coupling effect among multiple debris flows is always underestimated or ignored. It must be taken into consideration in the risk evaluation for post-seismic debris flows.

Conclusions

The Wenchuan earthquake produced an extraordinary amount of abundant loose materials that serve as potential debris source materials for subsequent rainfall-induced debris flow hazards. Numerous catastrophic debris flows have seriously threatened the local residents and facilities in the Wenchuan earthquake-stricken zones. In this study, adopting a soil-water

mixing model, coupled with a depth-integrated particle method, the post-seismic debris flows in the epicentral area of the Wenchuan earthquake are investigated based on satellite images. The debris source materials can be numerically investigated by assuming slope failure during the earthquake. The debris flow hazards in the epicentral area of the Wenchuan earthquake on 14 August 2010 are simulated in terms of volume, concentration, velocity, deposition thickness, discharge and affected area by setting cumulative rainfall, the Manning coefficient and the diffusion coefficient to 38 mm, 0.1 and 0.004 m^2 s^{-1}, respectively. The numerical results are well simulated and have good agreement with the actual debris flow hazards compared with field data in terms of the volume concentration, velocity, discharge and affected area, except the deposition thickness of debris flow, due to the volume of debris source materials being underestimated. Additionally, the coupling effect between multiple debris flows in both space and time increases the destructiveness of debris flows. Systematic analysis of the entire process of debris flow generation might contribute to understanding the mechanism of initiation, transportation and deposition, and be useful in designing effective protection structures according to the distribution characteristics of the main parameters.

References

Barnes H. (1967) Roughness characteristics of natural channels. Technical report USGS Water Supply Paper, 1967

Chen NS, Zhang F (2006) Movement and deposit characteristic of typical catastrophic debris flows by rainstorm in the mountainous area of southwestern China in 2003. Sci Geogr Sin 26(26):701–705 (in Chinese)

Chen HX, Zhang LM, Gao L, Yuan Q, Lu T, Xiang B, Zhuang WL (2016) Simulation of interactions among multiple debris flows. Landslides. https://doi.org/10.1007/s10346-016-0710-x

Chen C, Hawkins AB (2009) Relationship between earthquake disturbance, tropical rainstorms and debris movement: an overview from Taiwan. Bull Eng Geol Environ 68:161–186

Chow VT (1959) Open Channel Hydraulics. McGrawHill, New York

Crosta G (1998) Regionalization of rainfall thresholds: an aid to landslide hazard evaluation. Environ Geol 35(2–3):131–145

Donahue JL, Abrahamson NA (2014) Simulation-Based Hanging Wall Effects. Earthquake Spectra 30(3):1269–1284

Fei XJ, Shu AP (2004) Movement Mechanism and Disaster Control for Debris Flow. Tsinghua University Press, Beijing

Fan X, Xu Q, van Westen CJ, Huang R, Tang R (2017) Characteristics and classification of landslide dams associated with the 2008 Wenchuan earthquake. Geoenvironmental Disasters 4(1):12

Fan X, Juang CH, Wasowski J, Huang RQ, Xu Q, Scarinigi G, van Westen CJ, Havrnith HB (2018) What we have learned from the 2008 Wenchuan Earthquake and its aftermath: A decade of research and challenges. Eng Geol 241:25–32

Gorum T, Fan XM, Westen CJ, Huang HQ, Xu Q, Tang C, Wang G (2011) Distribution pattern of earthquake-induced landslides triggered by the 12 May 2008 Wenchuan Earthquake. Geomorphology 133:152–167

Gan JJ, Sun HY, Huang RQ (2012) Study on mechanism of formation and river blocking of Hongchungou giant debris flow at Yingxiu of Wenchuan county. Journal of Catastrophology 27(1):5–16 (in Chinese)

Ge YG, Chen XZ, Zhuang JQ, Zhu XH (2014) Characteristics, impacts and risks of dammed lakes induced by debris flows at the Wenchuan earthquake areas. Journal of Water Resource and Protection 6:1574–1588

Guo XJ, Cui P, Li Y, Zhang JQ, Ma L, Mahoney WB (2016) Spatial features of debris flows and their rainfall thresholds in the Wenchuan earthquake-affected area. Landslides 13:1215–1229

Huang RQ (2011) After effect of geohazards induced by the Wenchuan earthquake. J Eng Geol 19(2):145–151 (in Chinese)

Huang R, Fan X (2013) The landslide story. Nat Geosci 6:325–326

Huang RQ, Li WL (2009) Analysis of the geo-hazards triggered by the 12 May 2008 Wenchuan Earthquake, China. Bull Eng Geol Environ 68:363–371

Hungr O, Mcdougall S, Michael B (2005) Entrainment of Material by Debris Flows. Springer Praxis Books:135–158

Hürlimann M, Copons R, Altimir J (2006) Detailed debris flow hazard assessment in Andorra, a multidisciplinary approach. Geomorphology 78(3–4):359–372

Iverson RM (2014) Debris flows: behavior and hazard assessment. Geol Today 30(1):15–20

Iverson RM, Reid ME, Logan M, LaHausen RG, Godt JW, Griswold JP (2011) Positive feedback and momentum growth during debris-flow entrainment of wet bed sediment. Nat Geosci 4:116–121

Jeong S, Kim Y, Lee JK, Kim J (2011) The 27 July 2011 debris flows at Umyeonsan, Seoul, Korea. Landslides 12:799–813

Lan HX, Wu FQ, Zhou CH, Wang LJ (2003) Spatial hazard analysis and prediction on rainfall-induced landslide using GIS. Chin Sci Bull 48:703–708

Li DH, Xu XN, Hao HB (2012) Formation conditions and the movement characteristics of "8.14" giant debris flow in Yingxiu Town, Wenchuan County, Sichuan province. The Chinese Journal of Geological Hazard and Control 23(3):32–38 (in Chinese)

Limerinos J. (1970) Determination of the manning coefficient from measured bed roughness in natural channels. Technical Report, USGS Water Supply Paper, 1898-B

Lin CW, Shieh CL, Yuan BD, Shieh YC, Liu SH, Lee SY (2003) Impact of Chi-Chi earthquake on the occurrence of landslides and debris flows: example from the Chenyuan River watershed, Nantou, Taiwan. Eng Geol 71:49–61

Luna BQ, Remaitre A, Van Asch TWJ (2012) Analysis of debris flow behavior with a one dimensional run-out model incorporating entrainment. Eng Geol 128:63–75

McDougall S, Hungr O (2005) Dynamic modelling of entrainment in rapid landslides. Can Geotech J 42(5):1437–1448

Nakamura H, Tsuchiya S, Inoue K (2000) Sabo against Earthquakes. KokonShoin, Tokyo, pp 190–220

Nakata AM, Matsushima T (2014) Landslide simulation based on particle method: toward statistical risk evaluation. COMPSAFE 397–399

Okano K, Suwa H, Kanno T (2012) Characterization of debris flows by rainstorm condition at a torrent on the Mount Yakedake volcano, Japan. Geomorphology 136(1):88–94

Prochaska AB, Santia PM, Higgins JD, Cannon SH (2008) Debris-flow runout predictions based on the average channel slope (ACS). Eng Geol 98:29–40

Pastor M, Haddad B, Sorbino G, Cuomo S, Drempetic V (2009) A depth-integrated, coupled SPH model for flow-like landslides and related phenomena. Int J Numer Anal Methods Geomech 33:143–172

Pastor M, Blanc T, Haddad B, Petrone S, Sanchez MM, Drempetic V, Issler D, Crosta GB, Cascini L, Sorbino G, Cuomo S (2014)

Application of a SPH depth-integrated models to landslide run-out analysis. Landslides 11:793–812

Sepúlveda SA, Moreiras SM, Lara M, Alfaro A (2015) Debris flows in the Andean ranges of Central Chile and Argentina triggered by 2013 summer storms: characteristics and consequences. Landslides 12(1): 115–133

Takahashi T, Ashida K, Sawai K (1981) Delineation of debris flow hazard areas. Erosion and Sediment Transport in Pacific Rim Steeplands 132:589–603

Tan WP, Han QY (1992) Study on regional critical rainfall induced debris flow in Sichuan Province. Journal of Catastrophology 7:37–42 (in Chinese)

Tang C, Liang JT (2008) Characteristics of debris flows in Beichuan epicenter of the Wenchuan earthquake triggered by rainstorm on September 24, 2008. J Eng Geol 16(6):751–758 (in Chinese)

Tang C, Zhu J, Ding J, Cui XF, Chen L, Zhang JS (2011a) Catastrophic debris flows triggered by a 14 August 2010 rainfall at the epicenter of the Wenchuan earthquake. Landslides 8:485–497

Tang C, Li WL, Ding J, Huang XC (2011b) Field investigation and research on giant debris flow on August 14, 2010 in Yingxiu Town, epicenter of Wenchuan earthquake. Earth Science-Journal of China University of Geosciences 36(1):172–180

Tang C, Zhu J, Chang M, Ding J, Qi X (2012a) An empirical statistical model for predicting debris-flow runout zones in the Wenchuan earthquake area. Quat Int 250:63–73

Tang C, Van Asch TWJ, Chang M, Chen GQ, Zhao XH, Huang XC (2012b) Catastrophic debris flows on 13 August 2010 in the Qingping area, southwestern China: The combined effects of a strong earthquake and subsequent rainstorms. Geomorphology 139-140:55–576

Tang C, Jiang ZL, Li WL (2015) Seismic Landslide Evolution and Debris Flow Development: A Case Study in the Hongchun Catchment, Wenchuan Area of China. Engineering Geology for Society and Territory 2:445–449

Van Asch TWJ, Tang C, Zhu J, Alkema D (2014) An integrated model to assess critical rainfall thresholds for the critical run-out distances of debris flows. Nat Hazards 70(1):299–311

Xu Q, Zhang S, Li WL, Van Asch TWJ (2012) The 13 August 2010 catastrophic debris flows after the 2008 Wenchuan earthquake, China. Nat Hazards Earth Syst Sci 12:201–216

Xu C, Xu X, Yao X, Dai F (2014) Three (nearly) complete inventories of landslides triggered by the May 12, 2008 Wenchuan Mw 7.9 earthquake of China and their spatial distribution statistical analysis. Landslides 11:441–461

Zhang N, Matsushima T (2018) Numerical investigation of debris materials prior to debris flow hazards using satellite images. Geomorphology 308:54–63

Zhang N. (2015) Quantitative Evaluation of Debris Flow Hazard Using Depth-integrated Particle Method. Dissertation, University of Tsukuba

Zhang N, Matsushima T (2016) Simulation of rainfall-induced debris flow considering material entrainment. Eng Geol 214:107–115

Zhang S, Zhang LM, Lacasse S, Nadim F (2016) Evolution of Mass movements near epicenter of Wenchuan earthquake, the first eight years. Sci Rep 6:36154

Zhou W, Tang C (2014) Rainfall thresholds for debris flow initiation in the Wenchuan earthquake-stricken area, southwestern China. Landslides 11:877–887

Zhou W, Tang C, Van Asch TWJ, Zhou CH (2014) Rainfall-triggering response patterns of post-seismic debris flows in the Wenchuan earthquake area. Nat Hazards 70:1417–1435

Zhuang JQ, Cui P, Ge YG, Pei LZ (2009) Hazard assessment of debris flow valleys along Dujiangyan Wenchuan highway after '5.12' Wenchuan devastating earthquake. Journal of Sichuan University (Engineering Science Edition) 41(3):131–139 (in Chinese)